High temperature tribological performance of CrAlYN/CrN nanoscale multilayer coatings deposited on γ-TiAl

J. C. Walker[1*], I. M. Ross[1], C. Reinhard[2], W. M. Rainforth[1], P. Eh. Hovsepian[2]
[1]*University of Sheffield, Department of Engineering Materials, Sheffield, S1 3JD, UK*
[2]*Materials and Engineering Research Institute, Sheffield Hallam University, Sheffield, S1 1WB*
* Corresponding author: Tel: +44 151 794 5374, Fax: +44 151 794 4675, E-mail: john.walker@liverpool.ac.uk

Received Date Line (to be inserted by Production) (8 pt)

Abstract

Nanoscale multilayer nitride coatings deposited by advanced PVD techniques have shown particular promise in improving the tribological properties of a number of modal alloy steels [1]. In this study, we report the effect of temperature on the friction and wear behaviour of a CrAlYN/CrN multilayer coating with a CrAlYON/CrON topcoat deposited on γ-TiAl. Deposition was performed by unbalanced magnetron sputtering following a high power impulse magnetron sputtering (HIPIMS) pre-treatment of the polished substrate. A series of pin-on-disc type experiments, sliding against a polycrystalline alumina counterpart, were carried out at four temperatures: 20ºC, 120ºC, 300ºC and 650ºC. An increase in the average steady-state dynamic friction coefficient was observed between the material couple, from 0.56 at room temperature to 0.65 at 120ºC. However at higher test temperatures of 300ºC and 650ºC a decrease in these values was observed to 0.59 and 0.40, respectively. Scanning electron microscopy and energy dispersive X-ray analysis showed evidence of oxidation at the worn surface of all test temperatures investigated, whilst laser confocal microscopy indicated the formation of an interactive tribo-layer above the plane of the original test surface. Focused ion beam sectioning has been used to prepare site specific samples of the tribo-layers for transmission electron microscopy. The evolution of the wear scar composition and structure and its influence on the reduction in dynamic friction coefficient at elevated temperatures is discussed.

Keywords: Titanium aluminde; Nitride coating; Friction coefficient; Electron microscopy

1. Introduction

The combination of low density, good elevated temperature mechanical strength and excellent creep properties make γ-TiAl alloys attractive alternatives to conventional ferrous alloys for performance automotive components [2,3]. Such potential has already been demonstrated by the use of this material as exhaust values and turbocharger wheels [4,5], however further expansion into this and other markets, such as aerospace, has been somewhat limited by environmental and tribological degradation at elevated temperatures [5]. Efforts to improve both the low temperature ductility as well as high temperature environmental resistance of γ-TiAl initially centred

on processing and microstructural control [3,6], however in recent years the use of novel coatings deposited by physical vapour deposition (PVD) have emerged as an alternative means of protecting this alloy [7,8].

Nitride based monolithic surface coatings have been successfully applied as wear resistant coatings for the last 30 years, particularly for applications such as protection of tools steels during dry high speed machining [9]. Coating architectures have developed from the widespread use of the binary TiN coating to more elaborate multi-component systems which incorporate elements such as Al and C [1,9,10]. In recent years, multilayer coatings have also been developed in an effort to tailor the properties of thin individual layers specifically to the application in mind [11]. For example, the use of CrN and VN based multilayers has led to "super-hard" surface coatings which, whilst very effective at resisting surface abrasion, can also adapt their surface properties under certain tribological conditions to yield desirable friction behaviour [12-14].

This technology has now been applied to γ-TiAl substrates in an effort to introduce the alloy into environments currently precluded because of poor oxidation and tribological behaviour. Following successful application of wear resistant TiAlN/CrN based multilayer coatings to a number of high speed steel tool applications, a new system based on a CrAlYN/CrN multilayer structure has been developed and applied to γ-TiAl substrates [15]. Such titanium free coatings have been found to offer significant improvement in the oxidation protection at temperatures up to 850ºC [16]. The present study was concerned with assessing the tribological behaviour of a surface oxy-nitride layer as applied to the CrAlYN/CrN multilayer coating, sliding against an alumina counterpart over a range of temperatures from 20-650ºC. Extensive electron microscopy has been used to determine the surface interaction mechanisms as a result of elevated temperature and thus explain the observed frictional behaviour.

2. Experimental

2.1 Coating deposition

Substrate coupons of γ-TiAl alloy VBN-2 (nominal composition Ti-45Al-8Nb-0.17C at.%), obtained from GT Alloys, Nüremburg, Germany, were hand ground and polished to a 1μm diamond finish, prior to being mounted in the PVD deposition chamber. The machine utilises four stationary targets of either Cr, CrAlY or CrAl, with samples mounted on a three-fold planetary rotation system. Deposition of the multilayer structure was controlled by a number of process parameters including nitrogen partial pressure, sample rotation speed and target bias voltage. Comprehensive process details can be found elsewhere [15]. The surface of the γ-TiAl was etched using a high power impulse magnetron sputter (HIPIMS) technique, where Cr^+ ions were used to bombard the surface of the metal, resulting in both the etching and ion implantation in the upper sample surface. Following etching, a stress relieving CrAlN baselayer was deposited, approximately 1μm thick, followed by the deposition of the CrAlYN/CrN multilayer coating using the unbalanced magnetron sputtering mode of deposition. The processing parameters where adjusted to give a multilayer period of 3.1±0.1nm and a final coating thickness of 3.5μm. As a final stage, the partial pressure of oxygen in the coating chamber was increased in order to deposit an approximately 0.8μm thick oxy-nitride topcoat.

2.2 High temperature tribological testing

Surface profiles of the as-deposited coating were measured using a laser profilometer, and subsequent R_a values calculated, without any wavelength filters applied. Tribological testing was carried out using a CSM Instruments micro tribometer in a pin-on-disc configuration against a polycrystalline alumina ball (R_a=0.2µm) at four temperatures; room temperature (20ºC and 23%RH), 120ºC, 300ºC and 650ºC. Samples were allowed to heat to the test temperature for between 40 and 60 minutes. Tests were then run for 5000 revolutions using a normal contact load of 5N and a rotational speed of $1ms^{-1}$. Resistance to motion of the stationary alumina pin was logged and friction coefficients calculated for the test by the Tribolox software. The test run at room temperature was part of a larger testing program of different coatings, run for much longer sliding distances. As such, only the friction data for the first 5000 laps was comparable to the other higher temperature test samples.

2.3 Worn surface analysis

The worn surface of the test conducted at 120ºC was investigated by laser scanning confocal microscopy. An Olympus LEXT confocal microscope was used reconstruct the surface of the wear track. Profiles across the width of the track, perpendicular to the sliding direction, were also calculated. Raman microscopy of the worn surface of this sample was also undertaken using a Renishaw InVia system set up for green laser of 514nm wavelength at a power of 20mW. Traces were taken of both the un-worn coating as well as the wear debris present on the wear track. Due to the apparent damage of the wear debris by the laser, traces were acquired using only 10% of the laser intensity, in order to preserve the material structure.

Scanning electron microscopy was conducted on the worn surfaces of all coatings using a FEI Sirion FEG-SEM. The analysis was complemented by energy dispersive X-ray line and mapping analysis using an EDAX detector and Genesis software.

In order to further investigate the nature of the surface tribo-layer observed on the worn samples at room temperature, 300^{o}C and 650^{o}C, a FEI Quanta dual-beam focused ion beam (FIB) was used to prepare site-specific samples for transmission electron microscopy (TEM). The surface was protected using an in-situ deposited carbon film, initially using the electron beam, but later using the ion beam. Initial sectioning of the surface was undertaken using a 30kV Ga ion beam, with the voltage reduced to 5kV for final thinning. In-situ lift out of the TEM sample was undertaken using an Omniprobe™ micromanipulator. A Jeol 2010F TEM operating at 200kV was used to obtain bright and dark field images of the surface tribo-layer, whilst high angle annular dark field image (HAADF) scanning transmission electron microscope (STEM) images and EDX information further complimented the analysis. HAADF images are sensitive to atomic number, with higher z giving brighter contrast. In addition, electron energy loss spectroscopy (EELS) was used to determine the chemical composition and the local bonding state.

3 Results

3.1 Coating surface

The surface of the as-deposited CrAlYON/CrON coating was very uniform, Figure 1, with a low occurrence of growth defects. This was also reflected in the low surface roughness (R_a) value of 0.076µm, measured by laser surface profilometry.

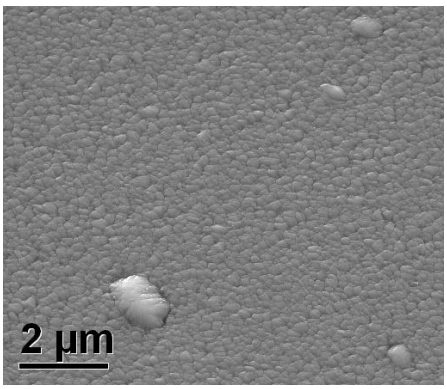

Figure 1. Secondary electron image of as deposited CrAlYON/CrON coating surface.

3.2 Friction coefficients

Average dynamic friction coefficients varied according to the test temperature, as indicated by Figure 2a) and b). Figure 2b) shows the relative difference in dynamic friction coefficient as a function of temperature. It was clear that the test conducted at 120ºC exhibited the highest average friction coefficient of 0.65 ± 0.03 (all error indicated represent one standard deviation), whilst the values for the room temperature and 300ºC test were similar at 0.56 ± 0.06 and 0.59 ± 0.04, respectively. After an initial run-in period, the test conducted at 650ºC showed the lowest average friction coefficient, 0.40 ± 0.03. Generally, the profile of all the friction coefficient curves exhibited an initial run-in period prior to the establishment of a constant average value. Small magnitude oscillations characteristic of stick-slip behaviour were most apparent during the room temperature test, and appear to reduce with increasing test temperature, such that the test at 650ºC exhibited almost a constant value of the friction coefficient for the majority of the test.

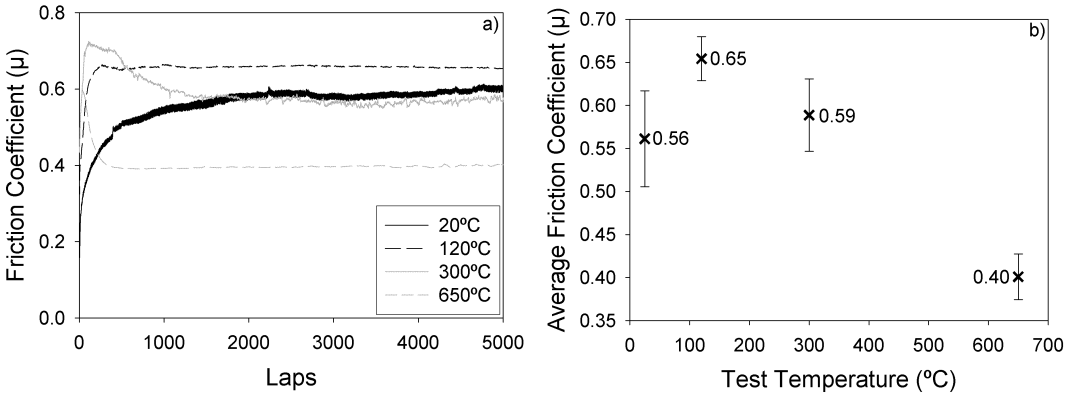

Figure 2. Variation of friction coefficient with sliding distance (a) and test temperature (b).

3.3 Worn surface topography

When imaged in the SEM all worn surfaces appeared extremely smooth. Figure 3 shows the room temperature worn surface. The worn surface itself appears relatively featureless, with some roughening at either side of the wear track. Closer examination, Figure 3b), showed that the roughening was associated with accumulated wear debris.

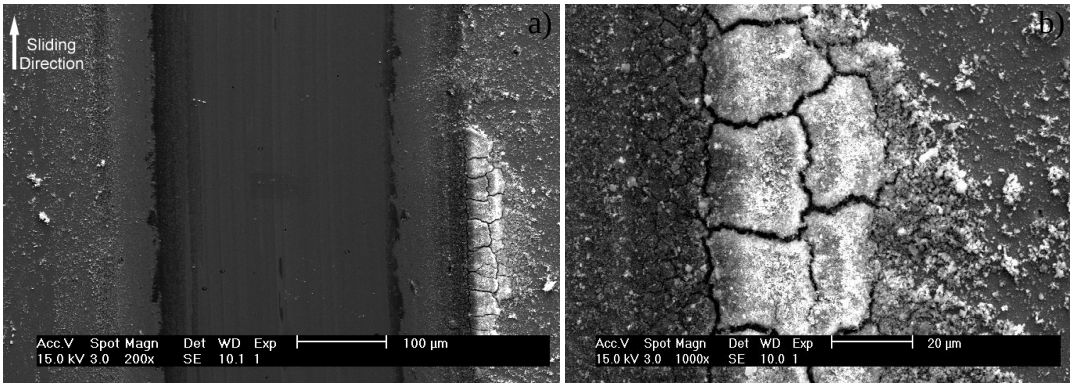

Figure 3. Secondary electron SEM images of the wear track at room temperature, showing the wear debris build up at the edges b), but an otherwise smooth wear track a).

Figure 4 shows the wear track at 120^{o}C, which was similar to that observed at room temperature. Figure 4b) shows an oxygen – Kα X-ray map of the same region, which suggests that the darker contrast in these former images (often found at the edge of the wear scar) correlates to the areas shown in the EDX map which are rich in oxygen. Figure 4c) gives an SEM image of the wear track which shows the build up of a tribolayer on the worn surface.

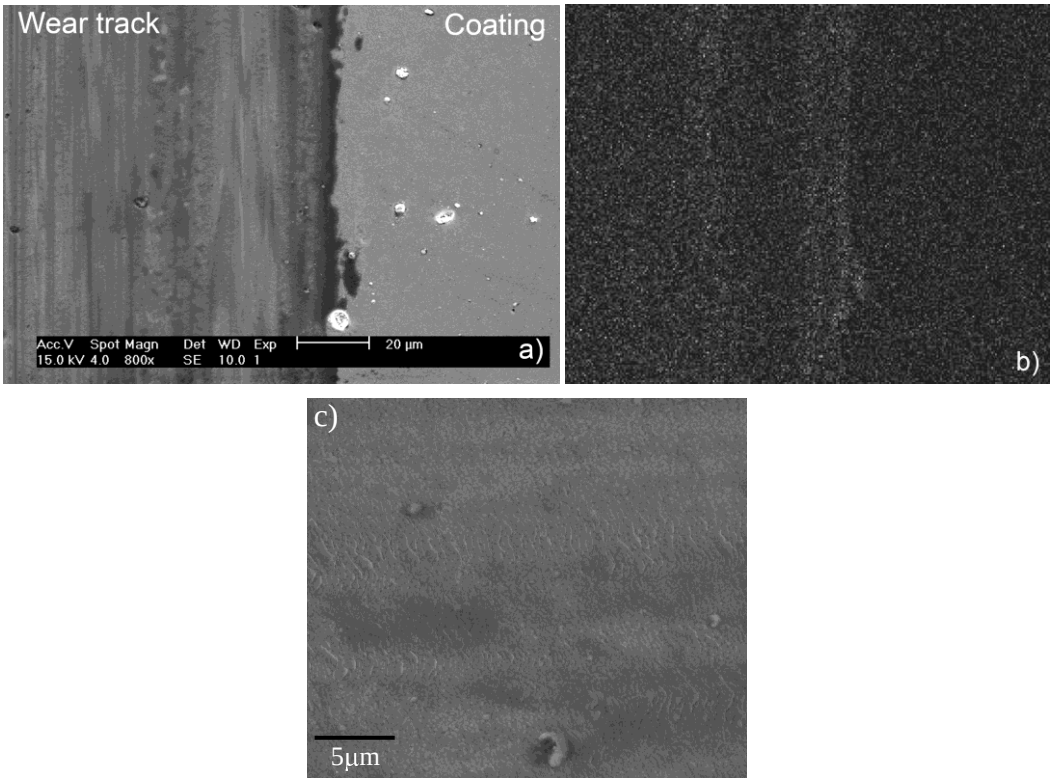

Figure 4. Secondary electron image (a) of the edge of the wear scar from 120ºC test and corresponding O-Kα EDX map (b). c) Higher magnification SEM image showing the surface layer build up.

SEM studies are excellent for a high lateral resolution studies of worn surfaces, but are not particularly sensitive to small differences in the z (height) direction due to the excellent depth of field in an SEM. Accordingly, laser scanning confocal microscopy was used to quantify the roughness of the wear scar. Figure 5 gives a laser confocal image of the wear scar from the test at 120ºC, with the corresponding 3-dimensional topographical surface reconstruction, shown in Figure 5b), of the same region. This indicated that much of the contacting asperities of the tribo-surface were actually raised above the plane of the original coating surface. This was confirmed in Figure 5c) which is a line profile across the width of the wear track, as indicated by the arrows in Figure 5a). There was an approximately 1-2µm increase in the height of the contacting asperities compared to level of the original oxy-nitride top-coat. Thus, it was not possible to make measurements of the volume loss and thus wear rates of these coatings, indicating that they were clearly extremely low.

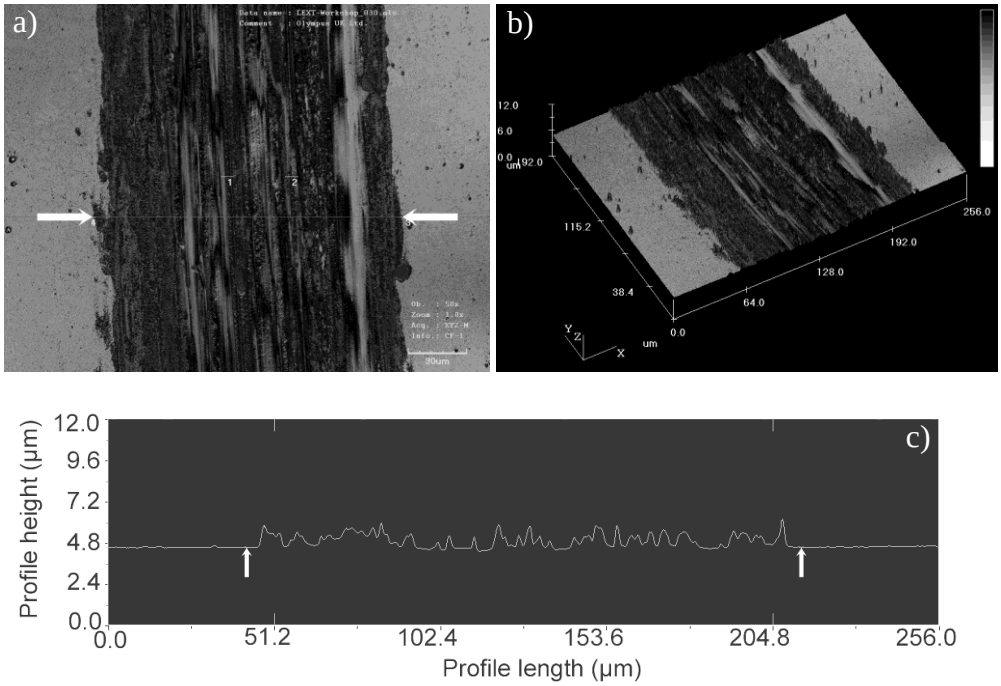

Figure 5. Optical micrograph (a) of the wear track from 120ºC test and corresponding 3D reconstruction (b) from laser confocal microscope. (c) A line profile between the points indicated in (a).

The wear scar at 300^{o}C exhibited a similar morphology to those at lower temperature, being generally smooth except at the edges of the wear track where the wear debris was accumulated, Figure 6. Surface analysis of the wear scar from the 650 ºC sample, Figures 7a,b) showed that the wear track appeared to be covered in a surface tribo-layer, which at certain points appeared to have fractured and been removed. EDX line analysis across a similar region of the wear scar, Figure 7c), showed that the oxygen Kα X-ray signal appeared to decrease in regions where fracture and removal of the surface tribo-layer had occurred. Indeed, the opposite was true for the nitrogen Kα X-ray signal which increased in such regions to a level similar to that observed on the un-worn coating surface. Signals for aluminium and chromium appeared constant across the line profile. Optical images of the alumina counterpart after the test at 650ºC, Figure 7d), clearly showed the initial contact region to the left of the image. The remainder of the contact surface appeared covered in the same tribo-layer as that observed on in the coating wear track, which was then subsequently smeared along the trailing edge of the alumina ball.

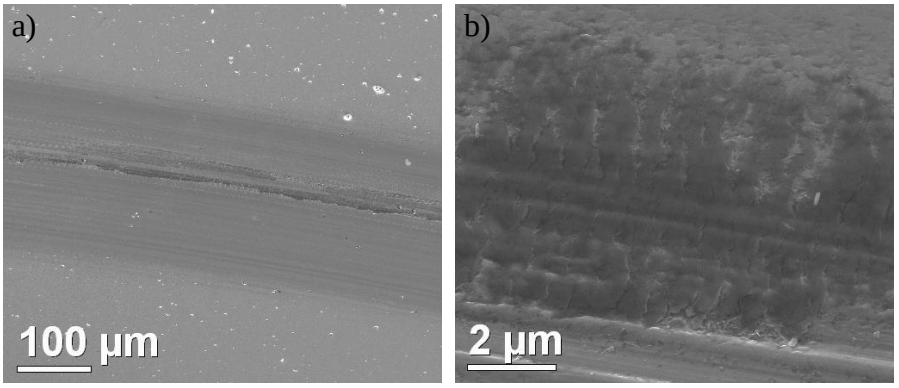

Figure 6. SEM secondary electron images of the worn surface at 300°C, which was generally smooth (a), except the wear debris build up at the edges (b).

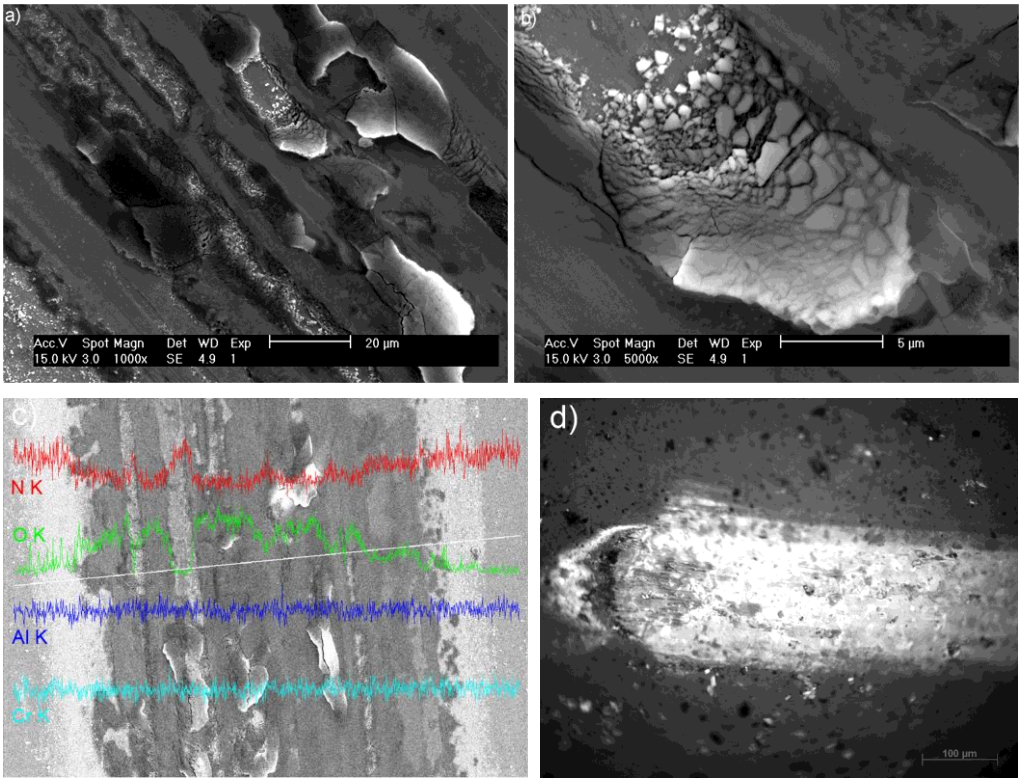

Figure 7. Secondary electron images (a & b) of the worn CrAlYN/CrN surface tested at 650ºC. (c) EDX line profiles across the wear track and (d) optical image of alumina counterpart ball after 650ºC test.

3.4 Raman microscopy

Optical microscopy of the 120ºC sample under bright field conditions, Figures 8a), showed two distinct areas with the wear scar; a high contrast area, similar in nature to the coating surface, as well as darker areas often at the edge of the wear scar. Whilst the higher contrast areas exhibited an identical Raman response as that observed

from the un-worn coating surface, Figure 8b), the darker areas displayed a series of new peaks at 560, 875 and 1005cm^{-1}.

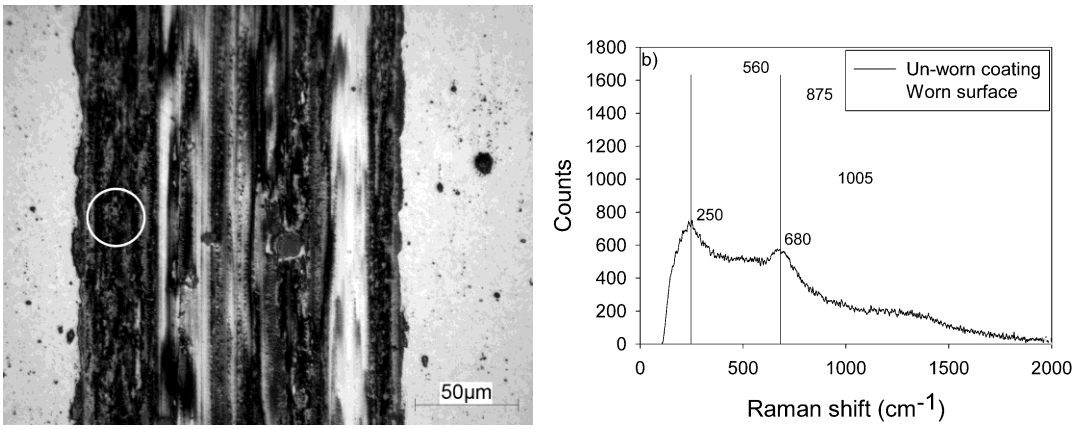

Figure 8. (a) Optical image of the wear scar. Raman spectra (b) from un-worn coating surface and region of wear scar indicated in (a).

3.5 Worn surface structure

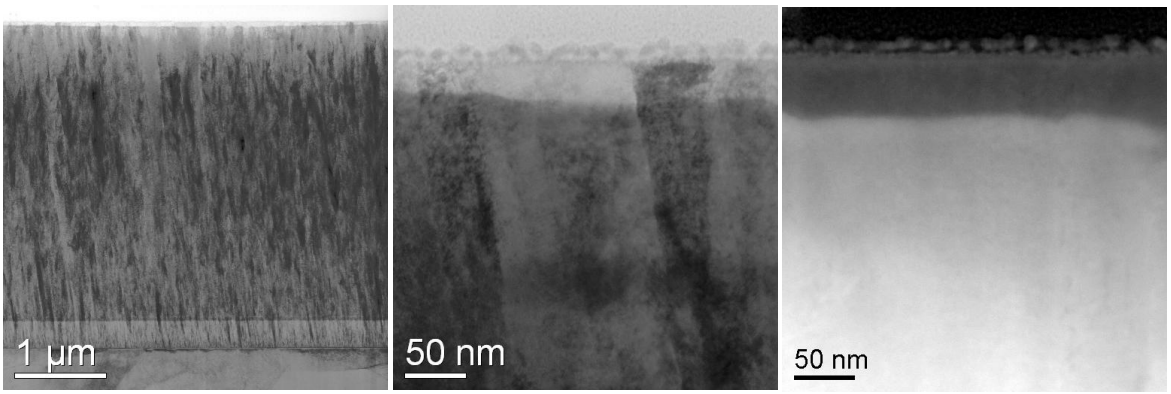

Figure 9. a, b) Bright field STEM images of a cross section of the worn surface from the room temperature test. a) gives an overview of the coating from substrate through to the worn surface. b) shows the worn surface itself, whilst c) is a HAADF STEM image of the same region.

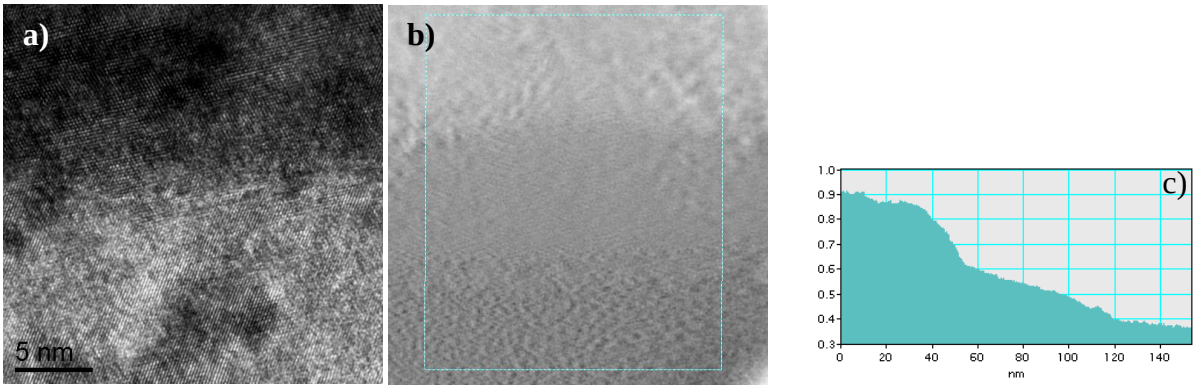

Figure 10. a) High resolution TEM of the region between the bright and dark areas in Figure 9c) (Note the sample is rotated by 180^{o} compared to Figure 9). b) Thickness map over the entire surface region, showing that the darker area in Figure 9c) is thinner than the coating below. c) Line scan trace showing the change in sample thickness. The y-axis indicates the thickness relative to the mean free path of electrons in this material, which is unknown.

Figure 9 gives STEM electron microscope images of the worn surface from the room temperature test. Figure 9a) shows the complete coating, from the γ-TiAl substrate (bottom), the bond coat and the coating itself through to the worn surface. No evidence of mechanical damage was found and indeed the surface was extremely smooth. A higher magnification image of the surface is given in Figure 9b) which shows an outer granular layer, comprising fine particles typically 10nm in diameter. The HAADF image in Figure 9c) gives atomic number contrast (darker regions have a lower atomic number), indicating that there was a surface layer below that had significantly different thickness or lower average atomic number than the coating. High resolution TEM of this layer indicated that it retained the coating crystalline structure, Figure 10a), although there was a distinct change in lattice fringe contrast in going from the brighter to the darker region in Figure 9c). Electron energy loss spectroscopy (EELS) indicated that the composition was the same in the outer dark layer as in the coating itself. Energy filtered TEM, which can be used to measure specimen thickness, indicated that the darker region was thinner than the brighter region, Figure 10b,c) but the difference was believed to be insufficient to explain the differences in contrast observed in Figure 9c).

Figure 11a) gives a bright field TEM image of the fine particles observed on the surface of the room temperature test, with Figure 11b) giving an energy filtered image showing the Cr distribution. Electron energy loss spectroscopy indicated that these particles had the same composition as the base coating, within experimental error. High resolution TEM failed to positively identify that they were crystalline. However, assuming the particles were spherical, given that the particles were ~10nm thick and embedded in a sample that was of the order ~100nm thick, the detection of lattice fringes would be unlikely. Therefore, it cannot be determined whether such particles were crystalline or not.

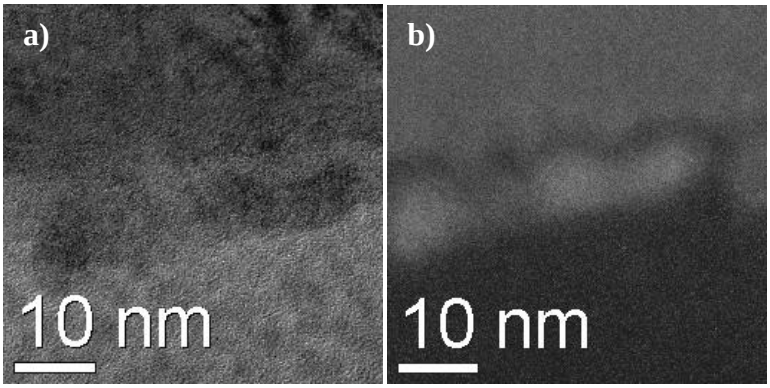

Figure 11. a) Bright field TEM image showing surface fine particles from the room temperature test (sample orientation that same as Figure 10). b) Energy filtered image of same area showing the Cr distribution.

Figure 12 gives STEM images of the worn surface at 300^{o}C. An immediately obvious difference to the surface structure at room temperature was the presence of cracks in two broad morphological categories: those that penetrated the entire coating and those that were largely confined to the oxynitride layer. The first type of cracks occurred at regular intervals along the surface. They generally penetrated the entire coating (although not always) and resulted in a local distortion of the substrate. The second type of crack was generally confined to the oxynitride outer layer, although some did locally penetrate further into the coating. The frequency of the second type of cracks was much greater than the first type. In addition to the cracking, an outer surface layer with lower average atomic number was observed, Figure 12c). This covered much of the surface and was morphologically very similar to that found at room temperature.

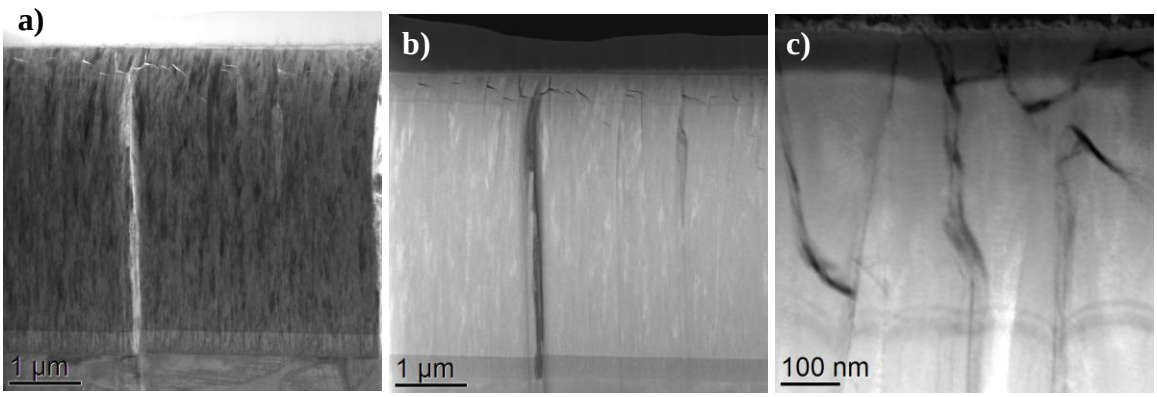

Figure 12. a) Bright field STEM image and b) corresponding HAADF image of the coating from substrate (bottom) through to the worn surface from the test at 300^{o}C. c) HAADF STEM image of the worn surface region, showing the cracks within the oxynitride layer.

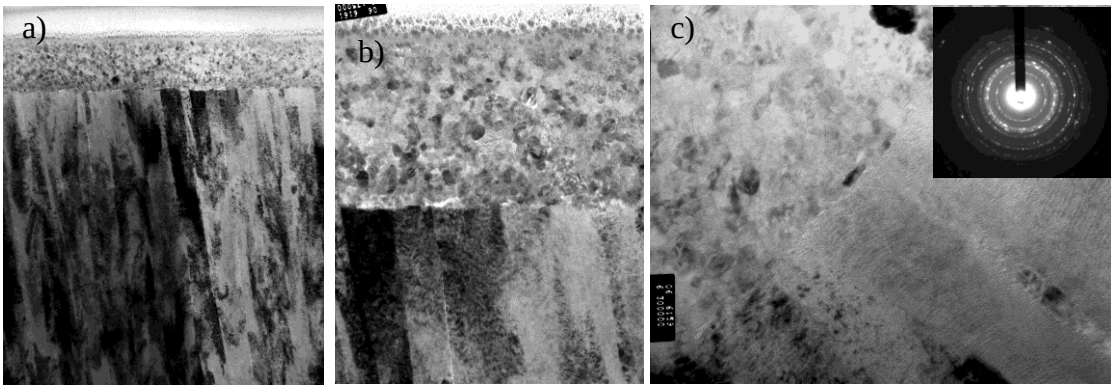

Figure 13. Bright field TEM micrographs of the worn surface for the test at 650°C. a) Section showing the coating and the outer tribolayer. b) Detail of the tribolayer, which appeared to have a finer grain structure at the outer regions compared to those closer in. c) Detail showing the interface between the tribolayer and the substrate, with selected area diffraction pattern of the tribolayer.

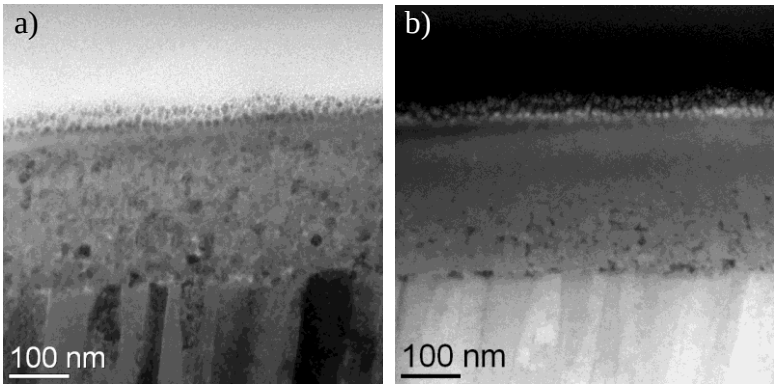

Figure 14. a) Bright field STEM image and b) HAADF image of the worn surface, from the test at 650°C, showing the tribolayer.

Figure 13 shows conventional bright field TEM images of the worn surface for the sample at 650°C. Figure 13a) shows an overview of the worn surface that exhibits a distinct tribofilm, of thickness around 400-500nm. Figure 13b) indicates that the layer comprises roughly equiaxed particles with grain size ~20-30nm. The inner region of the tribolayer appears relatively porous, but becomes finer and denser as the worn surface is approached. Figure 13c) shows the abrupt interface between the coating and the tribolayer. The inserted selected area diffraction pattern indicates that the tribofilm is crystalline and the nanocrystals have random orientation. The diffraction pattern could not be uniquely indexed, but does fit α-Al_2O_3, Cr_2O_3 or a mixture thereof. Figure 14 gives STEM images (bright field and HAADF) of the tribolayer. The HAADF image shows that the tribolayer had a lower average atomic number than the coating. In addition, it shows that the tribolayer did indeed become denser in going from the coating to the worn surface. The outer surface contained fine particles that were similar in size and morphology to those observed on the room temperature worn surface and which appeared to be fine, fragmented wear debris. This was consistent with the surface observations made with the SEM, Figure 7b).

4 Discussion

The trend of friction coefficient as a function of temperature exhibited similarities to tests for Ti based multilayer nitride coatings, but there were important differences. The steady state dynamic friction coefficient of this coating increased from 0.56 at room temperature to a maximum value of 0.65 at 120^{o}C. This is expected and is consistent with increases in friction coefficient with temperature for other ceramic materials [17,18]. Such phenomena are attributed to the removal of absorbed species such as water (which has been shown to reduce the friction coefficient between sliding alumina surfaces [18]) from the contacting surfaces. However, the friction coefficient then decreased when going from 120^{o}C to higher temperatures, which is the opposite trend to that seen in many nitride coatings. In general, friction is expected to increase as the hardness of the coating decreases with temperature rise. The one exception to this is the TiAlN/VN system, or other similar coatings containing appreciable amounts of V. As shown by Mayhofer et al. [19], and Zhou et al. [20], friction in this system tends to peak at 300^{o}C or thereabouts and then decreases, particularly in the region of >600^{o}C. In this case, Zhou et al. demonstrated that the lower friction was associated with the formation of vanadium based Magneli type phases, which are oxides of vanadium (e.g. V_2O_5), which have inherently low friction as a result of the low shear stress planes in the oxide. However, as demonstrated by Zhou et al., while the friction was low in this system, the wear rates at >600^{o}C were unacceptably high, and therefore such conditions result in rapid failure of the coating. Therefore, the results shown in the current work are relatively unique in as far as the coating produced both low friction and low wear (too low to measure for the test conditions used) at the high temperature of 650^{o}C. This is clearly a major technological advantage for the use of this coating.

The laser confocal microscopy indicated that the worn surface at 120^{o}C was higher than the surrounding coating, as a result of the build up of the surface. The profile across the wear track showed that the coating had not been penetrated as a result of the sliding action, but had in fact generated an intermediate tribo-layer between itself and the alumina counterpart. EDX mapping confirmed the presence of localised oxidation of the wear track. Raman spectroscopy of an area near the edge of the wear track showed a trace very similar to wear debris generated during the sliding of a CrN coating against alumina [21]. The presence of Al_2O_3 material was clearly demonstrated by the peaks at 875 and 1005cm^{-1} [10] and showed that transfer of counterpart material was contributing to the build up of the intermediate tribo-layer responsible for the higher friction coefficient. A weak peak observed at 560cm^{-1} was thought to be due to the initial formation of a Cr_2O_3 phase [10,21-23], however other peaks associated with this phase were not obvious.

The focused ion beam cross sections provide interesting insight to explain the trend in friction coefficient. At room temperature, the FIB sections revealed a smooth surface, consistent with the optical and SEM observations. No evidence of mechanical damage of the coating was found, which was consistent with the low wear rates. The only observable effect of the frictional contact was a thin layer of very fine particles, Fig. 9, typically of the order of 10nm in diameter. EELS demonstrated that these particles were essentially of the same composition as the coating. While the high resolution studies failed to show unequivocally that they were crystalline, this was

believed to be a limitation of imaging small (~10nm) particles in a thicker (~100nm) section. Indeed, occasional lattice fringes were observed. Therefore, the conclusion is that these particles were very fine wear debris particles that have remained attached to the surface.

The layer of darker contrast in Figure 9c) is harder to explain. The contrast in the HAADF image partly arises from this region being thinner than the coating below. FIB should provide a TEM sample of uniform thickness (and certainly no abrupt changes in thickness over a distance as small as 80nm) unless either the Ga ion beam has penetrated into the sample or where there is a significant difference in structure. TEM studies demonstrated that Ga had not penetrated this region; indeed the HAADF image would have been brighter had it done so. The high resolution and EELS studies did show that the darker region in Figure 9c) was crystalline and there was no fundamental change in structure or composition between this layer and the coating. Thus, the origin of this layer is difficult to explain, but the possibility that it is a preparation artefact cannot be ruled out.

The major difference in behaviour observed at 300^{o}C was extensive cracking. The through thickness cracks are characteristic of stick-slip behaviour or where significant deformation has occurred in the substrate. It would appear that the upper surface of the coating deformed plastically at this test temperature and this was believed to be a direct result of the combination of high friction and higher temperature leading to decreased mechanical properties. Such cracking, which ultimately leads to the failure of the coating, has been observed before at the same temperature but for TiAlN/VN on a stainless steel substrate, worn against the same counterface material[20]. In addition to the through thickness cracking, fine scale cracking was also observed in the surface of the coating. This appeared to be confined to the oxynitride region, which would be expected to be more brittle than the nitride substrate. Interestingly, the cracking had not resulted in any loss of the coating, from either the finer surface cracks or the through-thickness cracks. Thus, this did not represent failure of the coating. There was also no evidence of significant diffusion and oxidation of Ti or Al species from the substrate through the cracks. Such an effect had been observed on this coating at 850ºC [16], however it was clear that at 300ºC insufficient thermal energy was available to observe this effect.

Evidence from the worn surface of the coating tested at 650ºC indicated the formation of a tribo-layer, with distinct structure. Both SEM and FIB indicated that the outer part of this layer was denser and smooth on the surface as the result of sliding contact. However some areas, as shown in Figure 7b), showed evidence of delamination which was similar to an oxidational wear mechanism, where during mild wear, extremely smooth oxide plateaux form and eventually break up at a critical thickness [24]. EDX analysis and electron diffraction suggested that the layer was indeed a mixture of fine oxide particles. A unique identification of the surface layer was not made, but it appeared to be a mixture of alumina and chromia based oxides. Such a layer is often referred to as a glaze layer and is associated with low wear rates and steady, low friction values. The layer is similar to that observed by Zhou et al. [20] for TiAlN/VN, however, the big difference was that the wear rates for the CrAlYN/CrN were low, while for the TiAlN/VN, they were extremely high. Moreover, the layer in this case promoted low friction, where as equivalent surfaces for TiAlN based coatings tend to promote high wear rates at elevated temperature. Therefore, it would appear that the presence of chromium based oxides promotes low friction. This was consistent with studies on the room and elevated temperature dry sliding of self-mating plasma-

sprayed chromium oxide coatings [25] as well as TiN/CrN multilayer coatings sliding against an alumina counterpart [26].

The use of a Ti-free nano-scale multilayer coating has allowed the combination of low friction and low wear rates on a γ-TiAl substrate. The current work is the first to demonstrate that such a technologically important material can be protected at high temperature using a nitride coating, opening up the possibility of using this material in a variety of high temperature applications, including gas turbine engines.

5 Conclusions

1) CrAlYN/CrN multilayer coatings were successfully deposited onto γ-TiAl substrates and provided excellent protection against frictional contact.
2) Sliding wear tests against an alumina counterface produced wear rates that were too small to measure for the tests conditions used for temperatures up to 650^{o}C.
3) The friction coefficient increased from of 0.56 ± 0.06 at room temperature to a peak of 0.65 ± 0.03 at 120^{o}C, followed by a decrease with the lowest value of 0.40 ± 0.03 at 650^{o}C.
4) The only observable change in the surface structure for the room temperature test was a general smoothing of the original asperities, and a surface layer of very fine (~10nm) wear debris particles. The origin of an outer layer which exhibited dark contrast in HAADF images could not be uniquely identified.
5) At 120^{o}C, a distinct tribofilm was formed, which resulted in a rougher surface, consistent with the higher friction.
6) At 300^{o}C, fine surface debris particles were again observed. However, the coating contained through-thickness cracks that resulted in substrate distortion, and finer surface cracks, generally in the oxynitride surface layer. However, such cracks did not result in detachment or spalling of the coating. An outer layer which exhibited dark contrast in HAADF images which was morphologically similar to that at room temperature and could not be uniquely identified.
7) At 650^{o}C an outer layer of fine, equiaxed oxide particles (aluminium and chromium based) was formed, which constituted a glaze layer. The glaze layer was responsible for the low friction observed at this temperature.

Acknowledgements

The authors gratefully acknowledge the funding of the EU Framework 6 programme through the INNOVATIAL programme.

References

[1]P.E. Hovsepian, D.B. Lewis, Q. Luo, W.D. Munz, P.H. Mayrhofer, C. Mitterer, Z. Zhou, W.M. Rainforth, TiAlN based, nanoscale multilayer coatings designed to adapt their tribological properties at elevated temperatures, Thin Solid Films 485 (2005) 160-168

[2]C. Leyens, R. Braun, M. Frohlich, P.E. Hovsepian, Recent progress in the coating protection of gamma titaniumm aluminides, Jom 58 (2006) 17-21

[3]Y.W. Kim, Intermetallic alloys based on gamma titanium aluminde, Jom 41 (1989) 24-30

[4]W. Smarlsy, H. Baur, G. Glitz, H. Clemens, T. Kahn, M. Thomas, Titanium alumindes for automotive and gas turbine applications, TMS, Warrendale, PA, 2001

[5]C. Leyens, R. Braun, Environmental and thermal protection of high Nb-containing gamma titanium aluminides, Niobium: High Temperature Applications, Proceedings (2003) 239-251

[6]F. Appel, J.D.H. Paul, M. Oehring, C. Buque, Recent developments of TiAl alloys towards improved high-temperature capability, Gamma Titanium Aluminides 2003 (2003) 139-151

[7]R. Braun, M. Frohlich, W. Braue, C. Leyens, Oxidation behaviour of gamma titanium aluminides with EB-PVD thermal barrier coatings exposed to air at 900 degrees C, Surface & Coatings Technology 202 (2007) 676-680

[8]Z. Tang, F. Wang, W. Wu, Effect of a sputtered TiAlCr coating on hot corrosion resistance of gamma-TiAl, Intermetallics 7 (1999) 1271-1274

[9]W.D. Sproul, Multilayer, multicomponent and multiphase physical vapor-deposition coatings for enhanced performance, Journal of Vacuum Science & Technology A 12 (1994) 1595-1601

[10]H.C. Barshilia, K.S. Rajam, Raman spectroscopy studies on the thermal stability of TiN, CrN, TiAlN coatings and nanolayered TiN/CrN, TiAlN/CrN multilayer coatings, Journal of Materials Research 19 (2004) 3196-3205

[11]K. Holmberg, A. Matthews, H. Ronkainen, Coatings tribology - contact mechanisms and surface design, Tribology International 31 (1998) 107-120

[12]H.C. Barshilia, M.S. Prakash, A. Jain, K.S. Rajam, Structure, hardness and thermal stability of TiAlN and nanolayered TiAlN/CrN multilayer films, Vacuum 77 (2005) 169-179

[13]W.D. Munz, L.A. Donohue, P.E. Hovsepian, Properties of various large-scale fabricated TiAlN- and CrN-based superlattice coatings grown by combined cathodic arc-unbalanced magnetron sputter deposition, Surface & Coatings Technology 125 (2000) 269-277

[14]Z. Zhou, W.M. Rainforth, U. Falke, M. Falke, A. Bleloch, P.E. Hovsepian, On the structure and composition of nanoscale TiAlN/VN multilayers, Philosophical Magazine 87 (2007) 967-978

[15]P.E. Hovsepian, C. Reinhard, A.P. Ehiasarian, CrAlYN/CrN superlattice coatings deposited by the combined high power impulse magnetron sputtering/unbalanced magnetron sputtering technique, Surface & Coatings Technology 201 (2006) 4105-4110

[16]I.M. Ross, W.M. Rainforth, Z. Zhou, J.C. Walker, C. Reinhard, A.P. Ehiasarian, P.E. Hovsepian, R. Braun, C. Leyens, Oxidation characteristics of γ-TiAl-8Nb coated with a CrAlYN/CrN nanoscale multilayer coating, in Y. W. Kim, D. Morris, R. Yang and C. Leyens, TMS, TMS Warrendale, New Orleans, pp, 315-322

[17]R.H.J. Hannink, M.J. Murray, H.G. Scott, Friction and wear of partially stabilized zirconia - Basic science and practical applications, Wear 100 (1984) 355-366

[18]D.H. Buckley, Friction and wear behaviour of glasses and ceramics, Plenum, New York, 1974

[19]P.H. Mayrhofer, P.E. Hovsepian, C. Mitterer, W.D. Munz, Calorimetric evidence for frictional self-adaptation of TiAlN/VN superlattice coatings, Surface & Coatings Technology 177 (2004) 341-347

[20]Z. Zhou, W.M. Rainforth, P.E. Hovsepian, On the formation of tribofilms during the sliding wear of TiAlN/VN, Submitted to J. App. Phys. (2008)

[21]C.P. Constable, J. Yarwood, P. Hovsepian, L.A. Donohue, D.B. Lewis, W.D. Munz, Structural determination of wear debris generated from sliding wear tests on ceramic coatings using Raman microscopy, Journal of Vacuum Science & Technology A 18 (2000) 1681-1689

[22]H.Y. Chen, F.H. Lu, Oxidation behavior of chromium nitride films, Thin Solid Films 515 (2006) 2179-2184

[23]I.R. Beattie, T.R. Gilson, The single-crystal Raman spectra of nearly opaque materials. Iron (iii) oxide and chromium (iii) oxide, J. Chem. Soc. (A) (1970) 980-986

[24]T.F.J. Quinn, Review of oxidational wear .1. The origins of oxidational wear, Tribology International 16 (1983) 257-271

[25]Y.M. Zhou, R. Asaki, K. Higashi, W.H. Soe, R. Yamamoto, Sliding wear behavior of polycrystalline TiN/CrN multilayers against an alumina ball, Surface & Coatings Technology 130 (2000) 9-14

[26]H.S. Ahn, O.K. Kwon, Tribological behaviour of plasma-sprayed chromium oxide coating, Wear 225 (1999) 814-824